Composites: Part B 53 (2013) 112–120

Contents lists available at SciVerse ScienceDirect

Composites: Part B

journal homepage: www.elsevier.com/locate/compositesb

Homogenization of braided fabric composite for reliable large deformation analysis of reinforced rubber hose

J.R. Cho [a,b,*], Y.B. Jee [c], W.J. Kim [b], S.R. Han [d], S.B. Lee [a]

[a] School of Mechanical Engineering, Pusan National University, Busan 609-735, Republic of Korea
[b] Research & Development Institute of Midas IT, Gyeonggi-Do 463-400, Republic of Korea
[c] Narin Soft, Gyeonggi-Do 463-400, Republic of Korea
[d] Hwaseung R&A Co. Ltd., Gyeongnam 626-210, Republic of Korea

ARTICLE INFO

Article history:
Received 9 May 2012
Accepted 8 April 2013
Available online 25 April 2013

Keywords:
A. Fabrics/textiles
B. Mechanical properties
C. Finite element analysis (FEA)
D. Mechanical testing
Braided fabric composite

ABSTRACT

High pressure rubber hose is in the lamination structure composed of pure rubbers and braided fabric composite layers to have the sufficient strength against the excessive radial expansion and the large deformation, in which the braided fabric layer is woven with wrap and fill tows inclined to each other with the predefined helix angle in the complex periodic pattern. The consideration of detailed geometry of braided fabric layer in the numerical analysis leads to a huge number of finite elements so that the braided fabric layer has been traditionally simplified as an isotropic cylindrical one with the homogeneous isotropic material properties of braid spun tread. However, this simple model leads to the numerical prediction and design with the questionable reliability. In this context, this paper addresses the development of an in-house module, which is able to be interfaced with commercial FEM code, for the reliable large deformation analysis of the reinforced rubber hose with the element number at the level of the traditional simple model. The in-house module is able to not only automatically generate 3-D unit cell (or RVE) model of the braided fabric layer but evaluate the homogenized orthotropic material properties by automatically performing a serious of unit cell finite element analyses based on the superposition method. The validity of the in-house module and the reliability of the homogenization method are verified through the illustrative numerical experiments.

1. Introduction

High pressure rubber hoses are widely used in various engineering applications to convey gas, water and hydraulic oil. Power steering hose used in the automobile power steering system for mitigating the driver's steering force can be a representative example, which circulates the high-pressure hydraulic oil from the oil pump to the steering gear box [1,2]. In more severe situations, high pressure load is not static but periodically or randomly fluctuating, and furthermore thermal loading and large deformation are also coupled with the pressure load. Thus, high-pressure rubber hose should be designed to have the sufficient structural safety against leakage stemming from the excessive expansion, fatigue-induced microcracking and stress relaxation under such thermo-mechanical loading conditions [3–5].

High-pressure rubber hoses are generally in three- or five-layered lamination structure composed of pure rubbers and braided fabric layers, such that pure rubber layers resist leakage and chemical damage while the inserted braided fabric layers provide the sufficient strength against the large deformation of rubber hose. The braided fabric layer is in the complex periodic pattern composed of wrap and fill tows which are inclined to each other with the specific helix angle [6,7], so that the homogenized thermo-mechanical properties of the braided fabric layer are influenced by the braid structure as well as the material properties of base spun tread. However, the consideration of detailed geometry of braided fabric composite into the simulation model leads to a huge number of finite elements beyond the computation limit. For this reason, the braided fabric layers have been traditionally modeled as a simple homogeneous isotropic solid layer with the material properties of spun tread, resulting in the numerical analysis and design with the questionable reliability. A prominent geometric feature of the braided fabric layer is that the woven structure is periodic such that the representative volume element (RVE) is clearly defined, and this periodic structure allows one to homogenize the braided fabric layer once the homogenized material properties of RVE are obtained.

Regarding the homogenization methods for heterogeneous RVEs with regular or irregular morphologies, a significant body of

* Corresponding author. Address: School of Mechanical Engineering, Pusan National University, Busan 609-735, Republic of Korea. Tel.: +82 51 510 3088; fax: +82 51 514 7640.
E-mail address: jrcho@pusan.ac.kr (J.R. Cho).

1359-8368/$ - see front matter © 2013 Elsevier Ltd. All rights reserved.
http://dx.doi.org/10.1016/j.compositesb.2013.04.045

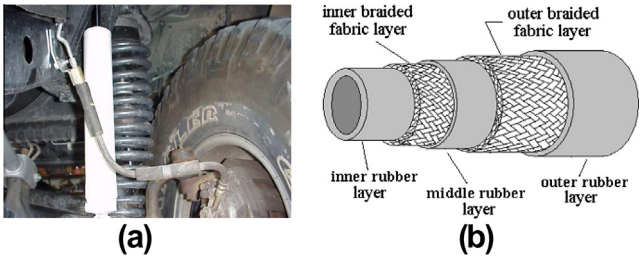

Fig. 1. (a) High pressure braking hose used in automobile and (b) its composition.

literature has been presented during several decades [8–11]. Among them, asymptotic expansion homogenization (AEH) [12,13] and superposition method [14,15] are widely used in computational mechanics for securing the numerical accuracy and the computational efficiency. Meanwhile, most efforts are focused on the computer-aided modeling of RVE for the numerical implementation of these homogenization methods. The geometric modeling techniques for complex heterogeneous RVEs can be classified into constructive and reconstructive approaches.

In the past few decades, RVEs composed of regular primitives such as triangle, square, rectangular, pentagonal or hexagonal cells have been constructed by the constructive approach making use of CAD tools and the packing of these unit cells. The objects with the periodic microstructure could be easily constructed by packing the unit cells in the regular pattern, but those are inherently difficult to modify the regularity and periodicity. In order to resolve the limitation of the regular packing, the stochastic packing approaches have been proposed [16,17]. Besides the constructive approaches, the reverse engineering based reconstructive approaches have

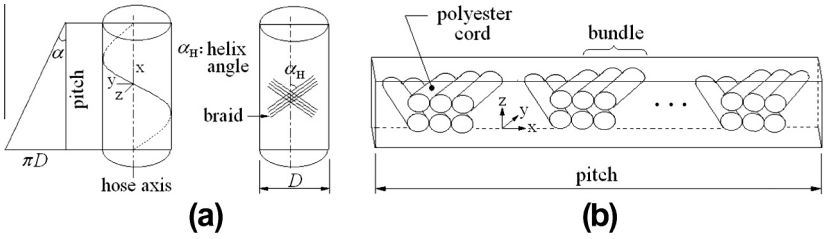

Fig. 2. (a) Helix angle and pitch and (b) cords and bundles.

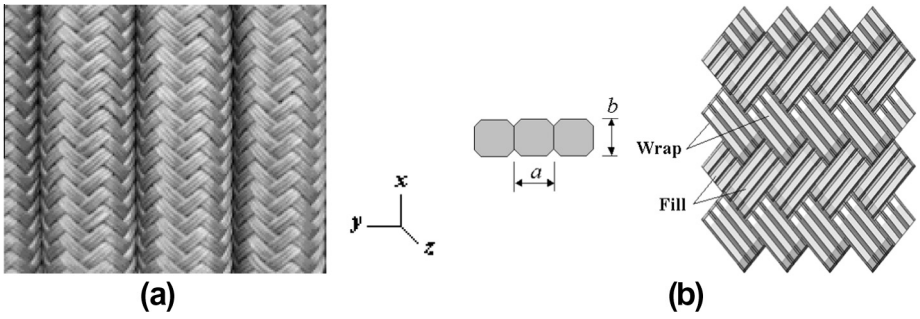

Fig. 3. (a) Unfolded real braided fabric layer and (b) 3-D CAD model of unit cell.

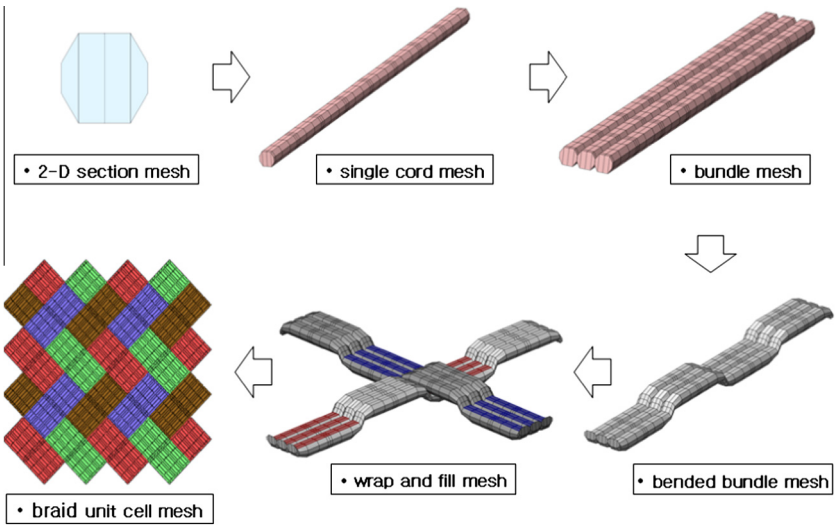

Fig. 4. Meshing procedure for unit cell of 3-D braided fabric composite.

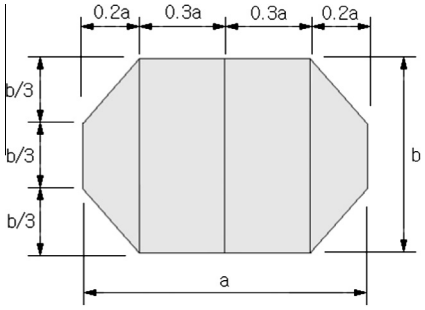

Fig. 5. Polygonal cross-section and dimensions of a braid cord.

been also extensively employed to generate nonperiodic random microstructures composed of irregular unit cells since the late 1990s. The random microstructure models can be reconstructed from a number of sources such as magnetic resonance imaging (MRI), scanning electron microscope (SEM), energy dispersive spectroscopy, Fourier transform IR spectroscopy, and X-ray computed tomography (CT) [18–20]. These reconstructed models can retain important features of realistic random microstructure geometry, curvature and roughness [21–23].

Braided fabric layer inserted in high pressure rubber hoses is in the 3-D complex woven structure such that the manual modeling job using commercial CAD tool becomes highly painstaking and time-consuming. In this context, this paper is concerned with the development of in-house module, which can be interfaced with commercial FEM code, for automatic solid modeling and mesh generation of RVEs of braided fabric layer and evaluating the homogenized orthotropic material properties by performing a serious of unit cell finite element analyses based on the superposition method. The validity of the in-house module and the reliability of the homogenization are verified through the illustrative numerical experiments.

2. Braided fabric layer of reinforced rubber hose

Fig. 1a shows a braking hose used in automobiles to convey high pressure hydraulic oil to the braking disk cylinders. It should satisfy the regularized high pressure-resisting structural strength and durability because oil leakage may lead to the fatal injury accident. Rubber hose intrinsically possesses high resistance against leakage and chemical reaction, but it may easily reach to the structural failure once the excessively large deformation is repeated during the steering operation subject to the pulsating internal oil pressure with high amplitude over 100 MPa. For this reason, high pressure rubber hose is reinforced by braided fabric layers inserted between pure rubber layers as represented in Fig. 1b. As a sort of laminated structure, braided fabric layers provide the mechanical strength against the pulsating pressure load while rubber layers resist the leakage and chemical reaction and protect the braided fabric layers from being torn and worn by the contact with other adjacent mechanical parts.

Braided fabric layer is woven with polyester or nylon cords by a special braiding machine such that wrap and fill tows cross each other with the predefined helix angle α_H. Referring to Fig. 2, bundles (called wrap or fill tows) composed of several cords are woven along the hose axis such that the preset number of bundles within a pitch, denoted by *Cr*, is periodically repeated. The diameter of braid cords is usually denoted by denia which is defined by the total weight in gram of braid cord per 9000 m. The effective mechanical properties of braided fabric composite are influenced by the helix angle, cord diameter and the braid structure as well as the material properties of base cords. Thus, both the numerical analysis accuracy and the design quality of the whole reinforced rubber hose are not guaranteed unless these design parameters are considered in the numerical simulation.

The configuration of the real unfolded braided fabric layer is shown in Fig. 3a, where each wrap and fill tow (bundle) is

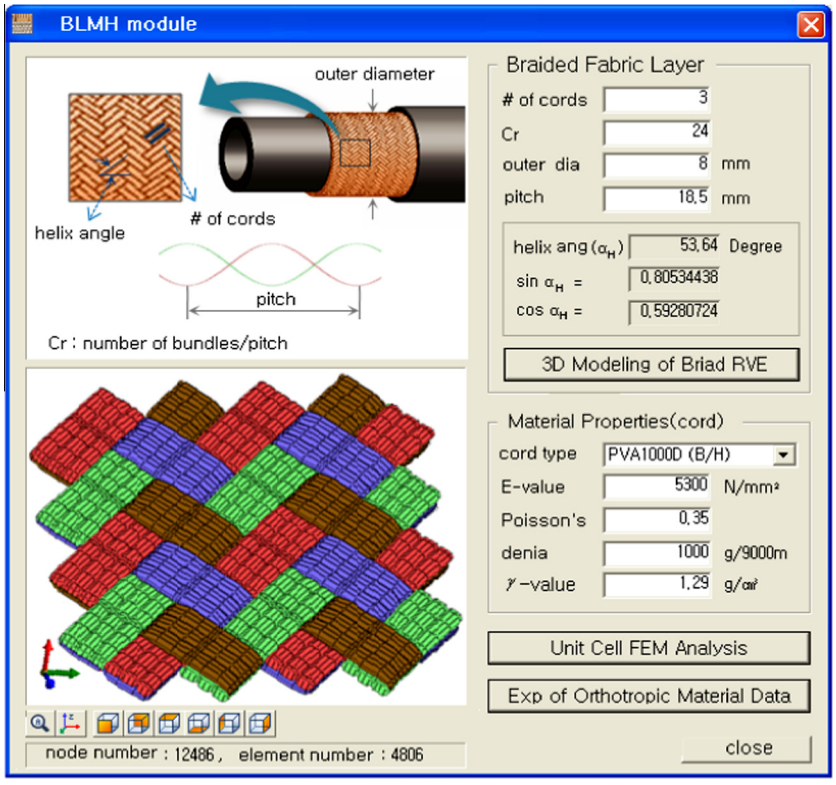

Fig. 6. GUI for the in-house module BLMH.

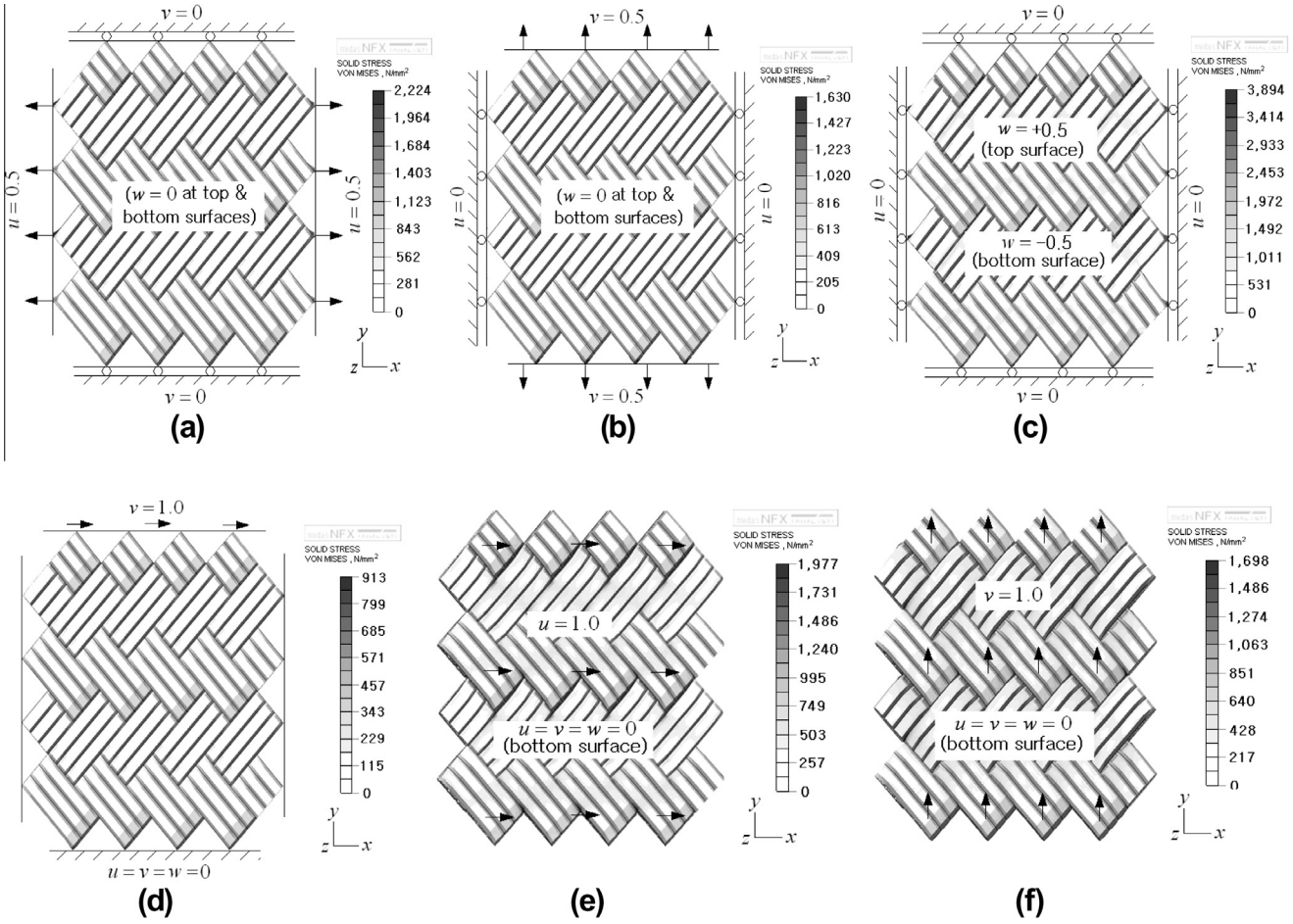

Fig. 7. Successive unit cell finite element analyses for outer braided fabric layer: (a) sub-problem 1, (b) sub-problem 2, (c) sub-problem 3 and (d–f) pure shear deformation for G_{12}, G_{23} and G_{31}.

composed of several polyester cords and a pitch contains twelve bundles in the axial direction of the hose. Since wrap and fill tows in the braided fabric layer are in the periodic structure, RVE (or unit cell) can be easily defined, differing from other heterogeneous phase composites. A unit cell taken for the 3-D detailed solid modeling and mesh generation is represented in Fig. 3b, where the sections of each wrap and fill tow are composed of those of cords in bundle and a and b are determined by the formulae given in Section 3.1. The finite element model is automatically generated with uniform 3-D hexahedron elements by our in-house module described in Section 3. The interfaces between wrap and fill tows are assumed to be completely bonded.

Referring to Figs. 2b and 3a, the Cartesian co-ordinates x, y and z are oriented such that y and z direct the hose axis and the thickness direction, respectively. When the braided fabric composite is assumed to be orthotropic, its constitutive relations are expressed in terms of the (6×6) stiffness matrix [24] which contains three Young's moduli E_1, E_2 and E_3, six Poisson's ratios $v_{ij}(i \neq j)$ and three shear moduli G_{23}, G_{13} and G_{12} such that

$$\begin{Bmatrix} \sigma_1 \\ \sigma_2 \\ \sigma_3 \\ \tau_{23} \\ \tau_{31} \\ \tau_{12} \end{Bmatrix} = \begin{bmatrix} \frac{1-v_{23}v_{32}}{E_2E_3\Delta} & \frac{v_{21}+v_{31}v_{23}}{E_2E_3\Delta} & \frac{v_{31}+v_{21}v_{32}}{E_2E_3\Delta} & 0 & 0 & 0 \\ \frac{v_{12}+v_{13}v_{32}}{E_3E_1\Delta} & \frac{1-v_{31}v_{13}}{E_3E_1\Delta} & \frac{v_{32}+v_{31}v_{12}}{E_3E_1\Delta} & 0 & 0 & 0 \\ \frac{v_{13}+v_{12}v_{23}}{E_1E_2\Delta} & \frac{v_{23}+v_{13}v_{21}}{E_1E_2\Delta} & \frac{1-v_{12}v_{21}}{E_1E_2\Delta} & 0 & 0 & 0 \\ 0 & 0 & 0 & G_{23} & 0 & 0 \\ 0 & 0 & 0 & 0 & G_{31} & 0 \\ 0 & 0 & 0 & 0 & 0 & G_{12} \end{bmatrix} \begin{Bmatrix} \varepsilon_1 \\ \varepsilon_2 \\ \varepsilon_3 \\ \gamma_{23} \\ \gamma_{31} \\ \gamma_{12} \end{Bmatrix} \quad (1)$$

with

$$\Delta = \frac{1 - v_{12}v_{21} - v_{23}v_{32} - v_{31}v_{13} - 2v_{12}v_{23}v_{31}}{E_1E_2E_3} \quad (2)$$

where subscripts 1, 2 and 3 stand for x, y and z respectively. From the symmetry of the compliance matrix, six Poisson's ratios satisfy $E_1v_{21} = E_2v_{12}$, $E_1v_{31} = E_3v_{13}$ and $E_3v_{23} = E_2v_{32}$. Hence, the total number of independent material constants to be determined is nine.

3. In-house module for evaluating the homogenized material properties

3.1. 3-D solid modeling and mesh generation of RVE

The mesh generation procedure of unit cell of 3-D braided fabric composite by utilizing the post-processor in midas NFX [25], commercial FEM software, is represented in Fig. 4. A straight single cord mesh is generated by extruding 2-D section mesh of braid cord in the cord axial direction, from which each bundle mesh is constructed by copying and bonding cord meshes. The cord length is determined by the number of cords in bundles and the number of bundles to be generated within unit cell, and the braid cord is uniformly discretized in the axial direction, except for the regions which are to be periodically bended to woven wrap and fill tows. The periodic bending of bundle meshes is constructed by extruding such cord regions up and down in the thickness direction. In this manner, a number of wrap and fill two meshes are copied, where the total of wrap and fill tows to be generated within unit cell. A

Table 1
Reaction forces and coefficients of three sub-problems for outer braided fabric layer.

Sub-problem	Reaction forces (N)			Coefficients ($\times 10^{-3}$)			
	F_x^i	F_y^i	F_z^i	Direction of P	α	β	γ
1	69.8518	3.7590	162.1253	x	14.791	−0.939	−0.283
2	3.7590	39.9907	117.5838	y	−0.846	25.661	−0.357
3	104.8064	64.5830	8077.0116	z	−0.185	−0.193	0.130

Table 2
Reaction forces and coefficients of three sub-problems for inner braided fabric layer.

Sub-problem	Reaction forces (N)			Coefficients ($\times 10^{-3}$)			
	F_x^i	F_y^i	F_z^i	Direction of P	α	β	γ
1	88.8784	3.5566	194.4186	x	11.600	−0.485	−0.245
2	3.5566	46.0580	134.6105	y	−0.427	22.300	−0.326
3	127.0047	77.6042	8963.5932	z	−0.161	−0.186	0.118

Table 3
Homogenized orthotropic material properties of outer and inner braided fabric layers.

Young's modulus (N/mm^2)			Poisson's ratio		
E_1	819.195	(915.340)[a]	ν_{12}	0.051	(0.032)[a]
E_2	733.147	(800.998)[a]	ν_{23}	0.157	(0.145)[a]
E_3	1128.406	(1547.103)[a]	ν_{31}	0.156	(0.179)[a]

[a] The homogenized material properties of the inner braided fabric layer.

3-D detailed unit cell mesh is finally generated by sequentially assembling the wrap and fill tow meshes.

The cross section of real braid cords is similar to lenticular shape, so it is modeled as a polygon using four 4-node quadrilateral elements as represented in Fig. 5, as close as possible to the real cross section. The width a of the polygonal cross section is determined by

$$a\ (\mathrm{mm}) = \frac{p}{C_r \times N_c} \tag{3}$$

with p and N_c being the pitch and the number of cords in each bundle. Meanwhile, the height b of the polygonal cross section is determined such that the specific weight of real braid cord, which is calculated using the information of denia, is conserved.

$$b\ (\mathrm{mm}) = \frac{denia/9 \times 10^6}{\gamma a(1 - 0.4/3)} \tag{4}$$

where γ (g/mm^3) and g (=9800 mm/s^2) are the specific weight of braid cord and the acceleration of gravity.

Fig. 6 shows a graphic user interface of in-house module called BLMH(braided layer material homogenization) developed for generating the 3-D unit cell mesh of braided fabric layer, performing the unit cell finite element analysis in sequence and calculating the homogenized orthotropic material properties by the superposition method. Once the geometry data of braided fabric layer is input, then a 3-D unit cell FEM model is automatically generated according to the above-mentioned meshing procedure and appears in the bottom window of GUI. The numbers of wrap and fill tows (bundles) within unit cell are commonly eight, so that the dimension of unit cell is dependent of the geometry data of cord and braided fabric layer. After that, six unit cell finite element analyses for three sub-problems and three pure shearing problems described in Appendix are automatically performed in sequence by midas-NFX, with the material properties input by user and the displacement conditions specified. The graphical numerical results of each unit cell analysis are sequentially displayed in the bottom window of GUI, and the homogenized orthotropic material properties are calculated according to the formulae given in Appendix and transformed into the (6 × 6) stiffness matrix defined in Eq. (1).

4. Numerical experiments

4.1. Homogenized orthotropic material properties of braided fabric layers

Referring to Figs. 1 and 2, inner and outer braided fabric layers woven with PVA (poly vinyl alcohol) are considered to illustrate the material homogenization using our in-house module. The material properties, the diameter D and the helix angle of the outer braid cords are as follows: E = 5300 N/mm^2, ν = 0.35, γ = 1.29 g/cm^3 (denia = 1000 g/9000 m), D = 8.0 mm and α_H = 53.64°, and each bundle contains three cords and the pitch p and C_r are set by 18.5 mm and 24, respectively. Meanwhile, the material properties, the diameter D and the helix angle of the inner braid cords are as follows: E = 6360 N/mm^2, ν = 0.35, γ = 1.29 g/cm^3 (denia = 1200 g/9000 m), D = 6.5 mm, α_H = 55.57°, and each bundle contains three

Table 4
Numerical results of the shear deformation analysis.

Plane	Shearing force P_s (N)	Shear strain γ_{ij}	Homogenized shear modulus G_{ij} (N/mm^2)
x–y	8.7861 (9.8733)	0.0133 (0.0139)	14.616 (17.818)
y–z	4825.8181 (4875.7085)	0.1499 (0.1370)	6490.833 (6832.693)
z–x	4917.4571 (4855.0396)	0.1499 (0.1370)	8241.512 (8816.179)

[a] The values of the inner braided fabric layer.

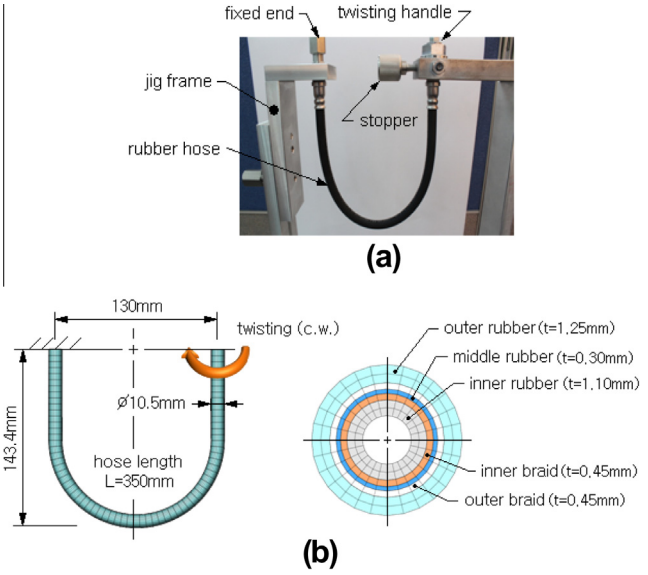

Fig. 8. Torsion of U-shaped reinforced rubber hose: (a) experiment apparatus and (b) finite element model.

Table 5
Moonley-Rivlin constants and bulk modulii of three rubber layers.

Rubber layer	C_{10}	C_{01}	D
Inner	0.58350	1.16111	1744.02150
Middle	0.13239	−0.12454	7.84270
Outer	0.99734	0.22850	1225.42264

cords and the diameter and the pitch p and Cr are set by 14.0 mm and 20, respectively.

The dimensions of the unit cell are as follows: $\Delta x = 6.012$ mm, $\Delta y = 7.491$ mm and $\Delta z = 0.662$ mm for the outer braided fabric layer and $\Delta x = 5.542$ mm, $\Delta y = 7.181$ mm and $\Delta z = 0.726$ mm for the inner braided fabric layer, respectively. The unit cell finite element meshes for the outer and inner braided fabric layers are equally composed of 4806 elements and 12,486 nodes. The displacement boundary conditions specified for each unit cell finite element analysis of the outer braided fabric layer are represented in Fig. 7a–e, together with the distributions of effective stress. The displacement boundary conditions are specified to the nodes being in contact with the planes indicated by the straight lines around the unit cells, and the reaction forces are also extracted in this manner. For the inner braided fabric layer, the unit cell finite element analyses are also carried out along the same procedure.

Referring to Fig. A1 in Appendix, the reaction forces acting on three faces of the unit cell which are obtained through the above-mentioned unit cell finite element analyses shown in Fig. 7a–c are given in Tables 1 and 2. Where, sub-problems 1, 2 and 3 indicate the unit cell finite element analyses Fig. 7a–c respectively, and superscripts i of the reaction forces refer to the number of sub-problems. According to Eq. (A1) in Appendix, together with nine reaction forces of three sub-problems, three sets of coefficients α, β and γ are calculated in sequence by letting $P = 1.0$ N at the top, middle and bottom of RHS of the matrix equation.

It is observed from the comparison of Tables 1 and 2 that the inner braided fabric layer produces higher reaction forces for all three sub-problems, which is consistent with the fact that the Young's modulus of the inner braided fabric layer is higher than the outer braided fabric layer. It is also observed that the reaction forces become highest in the z-direction and F_x^i and F_y^i show the remarkable difference in their magnitudes. The former informs that the stiffness of braided fabric layer in the thickness direction is higher than other two directions, and the latter is caused by the asymmetry of braided fabric layer composed of wrap and fill tows woven with the helix angle $\alpha \neq \pi/4$.

With the coefficients α, β and γ in Tables 1 and 2 and the uniform normal strains ε_{xx}^i, ε_{yy}^i and ε_{zz}^i obtained by the unit cell finite element analyses of three sub-problems, the homogenized Young's moduli and Poisson's ratios of the outer and inner braided fabric layers are calculated. The details on the calculation are described in Appendix, and the numerical results are given in Table 3. The inner braided fabric layer produces higher Young's moduli and smaller Poisson's ratios, except for ν_{31}, than the outer braided fabric layer. In both braided fabric layers, it is found that the Young's modulus is highest in the thickness direction and the in-plane Poisson's ratio is smallest.

Table 4 contains the numerical results associated with the evaluation of three homogenized shear moduli G_{23}, G_{31} and G_{12}. The detailed calculation procedure of the homogenized shear modulus is given in Appendix, and P_s and γ_{ij} in table are obtained by the unit cell finite element analyses Fig. 7c–e. In both braided fabric layers, the in-plane shear modulus G_{12} is found to be much smaller than other two out-plane shear moduli. Meanwhile, it is observed from the comparison between two braided fabric layers that the inner braided fabric layer shows higher shear moduli.

4.2. Large deformation analysis of the reinforced rubber hose

The large deformation analysis of the five-layered reinforced rubber hose is carried out to justify that the homogenized orthotropic material properties of braided fabric layers lead to more reliable numerical results. Fig. 8a shows a torsion test apparatus for U-shaped rubber hose, where the left end of the rubber hose is clamped while the right end is connected to the twisting handle. The U-shaped rubber hose undergoes the large deformation as its

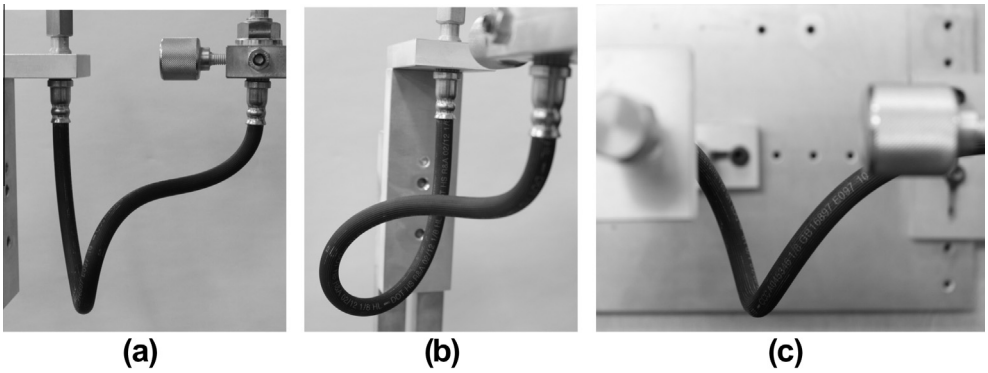

Fig. 9. Configuration of U-shaped reinforced rubber hose: (a) front view, (b) side view and (c) top view after twisted up to 180°.

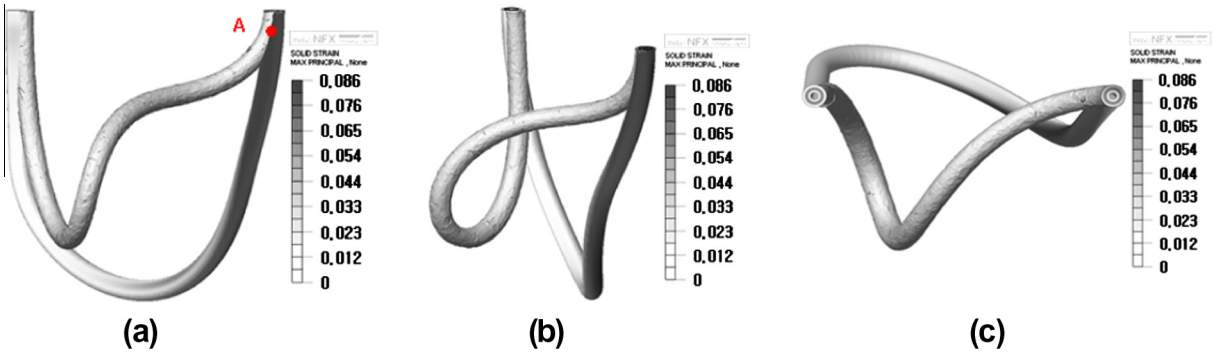

Fig. 10. Deformed configuration obtained using the homogenized isotropic model: (a) front view, (b) side view and (c) top view.

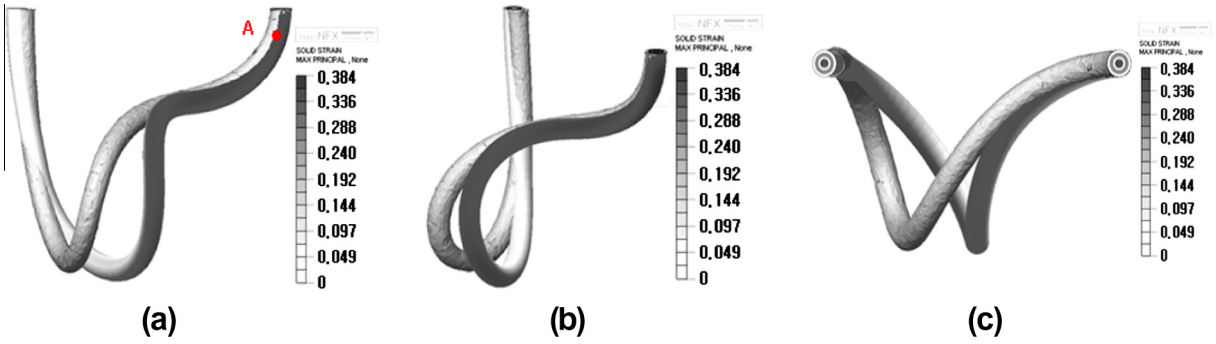

Fig. 11. Deformed configuration obtained using the homogenized orthotropic model: (a) front view, (b) side view and (c) top view.

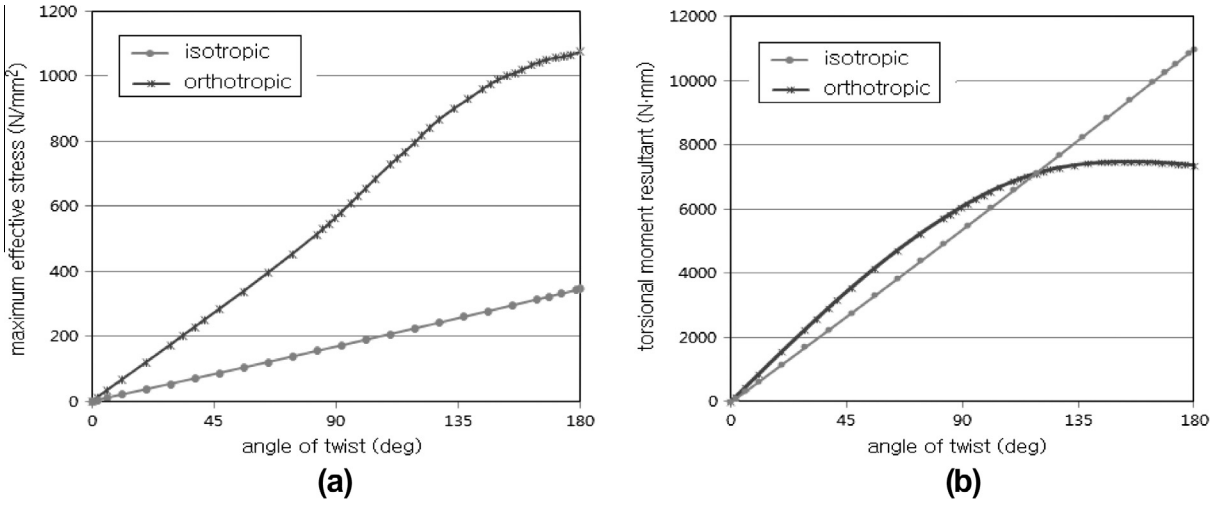

Fig. 12. Comparison of increment-histories between isotropic and orthotropic models: (a) maximum effective stress and (b) torsional moment resultant exerted on the twisting handle.

right end is forced to rotate clockwise up to 180°. The detailed dimensions of the rubber hose are given in Fig. 8b, and the torsional deformation is simulated with two different homogenized models for braided fabric layers, one is the homogenized orthotropic model and the other is the homogenized isotropic model. The material properties given in Tables 3 and 4 in the previous section are used for the homogenized orthotropic model, while E and v of braid cord are taken for the homogenized isotropic model.

Meanwhile, three rubber layers exhibit the incompressible hyperelastic behavior, so a five-term Moonley–Rivlin material model expressed by the strain energy density functional $W(I_1, I_2, I_3)$ given by

$$W = C_{10}(I_1 - 3) + C_{01}(I_2 - 3) + \frac{D}{2}(I_3 - 1)^2 \quad (5)$$

In which, I_i are the invariants of Green–Lagrange strain tensor, C_{ij} the material dependent Moonley–Rivlin constants, and D the bulk modulus to enforce the material incompressibility. The detailed numerical values of three material parameters for the inner, middle and outer rubber layers are given in Table 5. The entire rubber hose is uniformly discretized with the total of 16,129 8-node hexahedron elements, and the material nonlinear large deformation analysis is carried out by midas-NFX. The right end of rubber hose is twisted up to 180° during 100 increments according to Newton–Raphson method.

Fig. 9 represents three different views of the deformed configuration of the rubber hose after the twisting handle is rotated clockwise up to 180°. It is clearly observed that the reinforced rubber hose is significantly deformed to the left and upper direction. The deformed configuration obtained by experiment is used as the reference solution for the comparison of the numerical results between the above-mentioned two different simulation models.

Three different views of the deformed configuration of the rubber hose which are obtained using the homogenized isotropic model are represented in Fig. 10, where the digital images captured at experiment are also included for better comparison. One can clearly observe the big discrepancy between two deformed configurations, because the numerically predicted one is much smaller so that the remarkable large deformation to the left and upper direction is not clearly apparent. However, differing from the homogenized isotropic model, the homogenized orthotropic model shows the deformed configuration close to one obtained by experiment, as shown in Fig. 11. The large deformation to the left and upper direction is clearly observed, and the maximum principal strain is almost four and half times as high as one predicted by the homogenized isotropic model. Therefore, it has been clearly justified that the homogenized orthotropic model leads to more accurate numerical result of the large deformation of the reinforced rubber hose.

Fig. 12a and b represent the increment-histories of the maximum effective stress and the torsional moment resultant exerted on the twisting handle. The maximum effective stress is occurred at point A. Both quantities predicted by the homogenized isotropic model increase linearly with the angle of twist, differing from the homogenized orthotropic model showing the inherent nonlinear increment-histories. It can be found from the comparison of the deformed configurations that the homogenized isotropic model is stiffer, which can also be explained from the comparison of the maximum effective stresses and the torsional moment resultants at the final stage. Thus, it has been found that the isotropic homogenization cannot appropriately model the highly direction-dependent stiffness of braided fabric layer.

5. Conclusion

An in-house module for evaluating the homogenized orthotropic material properties of braided fabric layers inserted in reinforced rubber hose has been developed and interfaced with commercial FEM software. The in-house module is composed of three parts, automatic solid modeling and mesh generation of unit cell of braided fabric composite, performing a sequence of unit cell finite element analyses, and computation of the homogenized orthotropic mechanical properties of braided fabric layer by the superposition method. It has been verified through the illustrative numerical experiment that the in-house module automatically generated 3-D unit cell finite element models of complex braided fabric layers and successfully calculated the homogenized orthotropic material properties by carrying out a sequence of unit cell finite element analyses.

The evaluated homogenized material properties have been applied to the torsional large deformation analysis of a U-shaped five-layered reinforced rubber hose. For the comparison purpose, the torsion experiment and the numerical simulation using the homogenized isotropic model were also performed. The homogenized isotropic model produced the over-stiffened small deformation with the significant discrepancy from the experimental result, but the homogenized orthotropic model showed the deformed configuration close to one at experiment. It has been justified from the comparative experiment that the orthotropic homogenization can appropriately model the direction-dependent stiffness of braided fabric layer. Furthermore, it is convinced that the in-house module interfaced with commercial FEM software could be a useful tool for the reliable large deformation analysis and design of reinforced rubber hoses used in various engineering fields.

Acknowledgements

The financial support for this work through World Class 300 from Ministry of Knowledge Economy of Korea is gratefully acknowledged. The financial support given to one of authors (S.B. Lee) by Pusan National University under the independent academic research fund (2 years) is gratefully acknowledged.

Appendix A1. Superposition method

Referring to Fig. A1, a unidirectional uniform tension of the unit cell by the external load P can be decomposed into a linear combination of three sub-problems. In sub-problem 1, two surfaces facing to the x-direction are subject to uniform displacement u but the other four surfaces are clamped. Then, the force resultants F_x^1, F_y^1 and F_z^1 exerted on all the surfaces and the normal stains $\varepsilon_{xx}^1, \varepsilon_{yy}^1$ and ε_{zz}^1 produced in the unit cell can be computed by the unit cell finite element analysis, where the superscript 1 stands for the sub-problem 1. Meanwhile, sub-problems 2 and 3 are defined by changing two displacement- and four fixed-boundary surfaces and the corresponding force resultants and the normal strains can be computed by the unit cell finite element analysis (see Fig. A1).

Three coefficients α, β and γ in the linear combination of sub-problems can be determined from the static equivalence between the original and decomposed problems:

$$\begin{bmatrix} F_x^1 & F_x^2 & F_x^3 \\ F_y^1 & F_y^2 & F_y^3 \\ F_z^1 & F_z^2 & F_z^3 \end{bmatrix} \begin{Bmatrix} \alpha \\ \beta \\ \gamma \end{Bmatrix} = \begin{Bmatrix} P \\ 0 \\ 0 \end{Bmatrix} \tag{A1}$$

Then, three uniform normal strains ε_1, ε_2 and ε_3 appeared in the original problem are calculated as

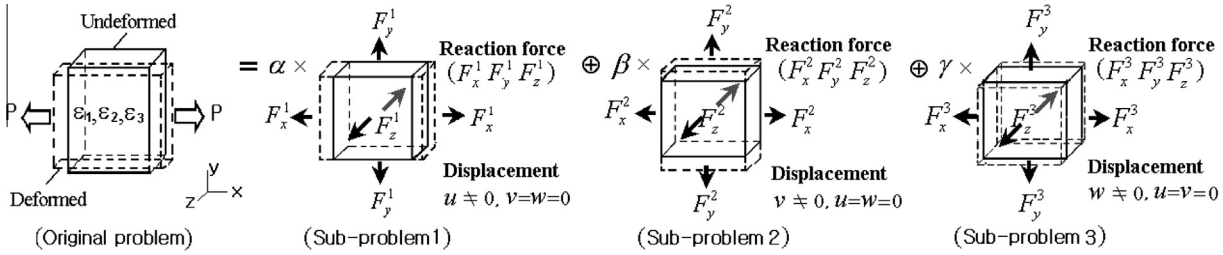

Fig. A1. Superposition method (original and decomposed problems).

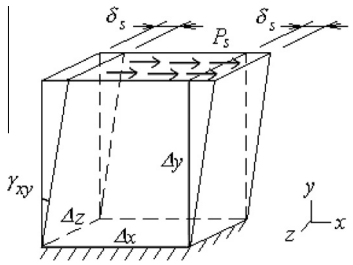

Fig. A2. A unit cell under the pure shear deformation.

$$\varepsilon_1 = \alpha\varepsilon^1_{xx}, \varepsilon_2 = \beta\varepsilon^2_{yy}, \varepsilon_3 = \varepsilon^3_{zz} \tag{A2}$$

And the homogenized Poisson's ratio v_{12} of the braided fabric composite is determined from

$$v_{12} = -\varepsilon_2/\varepsilon_1 = -\beta\varepsilon^2_{yy}/\alpha\varepsilon^1_{xx} \tag{A3}$$

On the other hand, the work W done by the uniform external load P and the internal strain energy U stored in the original problem are calculated by

$$W = Pu/2 = P(\varepsilon_1\Delta x)/2 \tag{A4}$$

$$U = \frac{1}{2}\int_V \sigma_1\varepsilon_1 dV = \frac{1}{2}E_1(\varepsilon_1)^2\Delta x\Delta y\Delta z \tag{A5}$$

Equating U with W, one can obtain the homogenized Young's modulus E_1 of the braided fabric composite given by

$$E_1 = \frac{P}{(\Delta x\Delta y)\varepsilon_1} = \frac{P/\alpha}{(\Delta x\Delta y)\varepsilon^1_{xx}} \tag{A6}$$

In this manner, the remaining four homogenized mechanical properties E_2, E_3, v_{23} and v_{13} can be determined by applying the uniform external load P to the original problem in the y- and z-direction respectively. There is no change for defining the corresponding sub-problems, but P in Eq. (A1) should be moved to the second and the third row to calculate coefficients α, β and γ. The calculation of the homogenized Poisson's ratios v_{23}, v_{31} and Young's moduli E_2, E_3 are straightforward from Eqs. (A2), (A3), (A4), (A5), (A6).

Fig. A2a shows a unit cell subject to a uniform horizontal displacement δ_s on the upper surface with the bottom surface clamped. Then, the shearing force P_s exerted on the upper surface can be obtained by the unit cell finite element analysis, and the shear strain $\gamma_{xy} = \gamma_{12}$ is calculated by dividing δ_s by the height of unit cell. The external work done and the internal strain energy by the shearing force are as follows:

$$W = P_s\delta_s/2 = P_s\gamma_{xy}\Delta y, \quad \gamma_{xy} \cong \delta_s/\Delta y \tag{A7}$$

$$U = \frac{1}{2}\int_V \tau_{12}\gamma_{12}\, dV = \frac{1}{2}G_{12}(\gamma_{12})^2\Delta x\Delta y\Delta z \tag{A8}$$

By equating both quantities gives us the homogenized shear modulus G_{12} given by

$$G_{12} = P_s/\gamma_{12}(\Delta x\Delta y) \tag{A9}$$

In the same manner, the remaining homogenized shear moduli G_{23} and G_{13} can be determined by changing the clamped and loading surfaces.

References

[1] Nishimura S, Matsunaga T. Analysis of response lag in hydraulic power steering system. JSAE Rev 2000;21:41–6.
[2] Cho JR, Song JI, Noh KT, Jeon DH. Nonlinear finite element analysis of swaging process for automobile power steering hose. J Mater Process Technol 2005;170:50–7.
[3] Entwistle KM. The behavior of braided hydraulic hose reinforced with steel wires. Int J Mech Sci 1981;23:229–41.
[4] Kwak SB, Choi NS. Micro-damage formation of a rubber hose assembly for automotive hydraulic brakes under a durability test. Eng Fail Anal 2009;16(4):1262–9.
[5] Cho JR, Song JI. Swaging process of power steering hose: its finite element analysis considering the stress relaxation. 2007;187–188:497–501.
[6] Tabiei A, Ivanov I. Computational micro-mechanical model of flexible woven fabric for finite element impact simulation. Int J Numer Methods Eng 2002;53:1259–76.
[7] Bendsøe, Kikuchi N. Generating optimal topologies in structural design using homogenization method. Comput Methods Appl Mech Eng 1998;71:197–224.
[8] Bensoussan A, Lions JL, Papanicolaou G. Asymptotic analysis for periodic structures. Amsterdam: North-Holland Publishing Company; 1978.
[9] Sanchez-Palencia E. Non-homogeneous media and vibration theory. Lecture Notes in Physics; 1980. p. 127.
[10] Reiter T, Dvorak GJ. Micromechanical models for graded composite materials: II. Thermomechanical loading. J Phys Solids 1998;46(9):1655–73.
[11] Cho JR, Oden JT. Functionally graded materials: a parametric study on thermal stress characteristics using the Crank–Nicolson–Galerkin scheme. Comput Methods Appl Mech Eng 2000;188:17–38.
[12] Chung PW, Tamma KK, Namburu RR. Asymptotic expansion homogenization for heterogeneous media: computational issues and applications. Composites Part A: Appl Sci Manufact 2001;32(9):1291–301.
[13] Vel SS, Goupee AJ. Multiscale thermoelastic analysis of random heterogeneous materials, part I: microstructure characterization and homogenization of material properties. Comput Mater Sci 2010;48:22–38.
[14] Kato T, Nishioka T. Analysis of damaged material containing periodically distributed elliptical microcracks by using the homogenization method based on the superposition method. Int J Fract 2002;115(4):305–21.
[15] Cho JR, Kang YJ, Jeong KY, Noh YJ, Lim OK. Homogenization and thermoelastic analysis of heterogeneous materials with regular and irregular microstructures. Composites: Part B 2013;43:2313–2323.
[16] Cho JR, Song JI, Choi JH. Prediction of effective mechanical properties of reinforced braid by 3-D finite element analysis. vol. 306–308. Key Eng Mater; 2006. p. 799–804.
[17] Schroeder C, Regli WC, Shokoufandeh A, Sun W. Computer-aided design of porous artifacts. Comput Aided Des 2005;37(3):339–53.
[18] Luchnikov VA, Medvedev NN, Oger L, Troadec JP. Voronoi–Delaunay analysis of voids in systems of nonspherical particles. Phys Rev E 1999;59(6):7205.
[19] Rigby SP, Gladden LF. NMR and fractal modeling studies of transport in porous media. Chem Eng Sci 1996;51(10):2263–72.
[20] Wong KH, Davis TP, Barner-Kowolik C, Stenzi MH. Honeycomb structured porous films from amphiphilic block copolymers prepared via the RAFT process. Polymer 2007;48(10):4950–65.
[21] Paquet D, Ghosh S. Microstructural effects on ductile fracture in heterogeneous materials. Part I: sensitivity analysis with LE-VCFEM. Eng Fract Mech 2011;78(2):205–25.
[22] Virnovsky GA, Lohne A, Frette OI. Modeling capillary pressure using capillary bundles with arbitrary cross-section obtained from photomicrograph. J Petrol Sci Eng 2009;69(1-2):117–28.
[23] Tsakiroglu CD, Ioannidis MA, Amirtharaj E, Vizika O. A new approach for the characterization of the pore structure of dual porosity rocks. Chem Eng Sci 2009;64(5):847–59.
[24] Daniel IM, Ishai O. Engineering mechanics of composite materials. New York: Oxford University Press; 1994.
[25] Midas IT, Users' Manual of midas NFX. Gyeonggi: Midas IT; 2011.